High Specific Capacity Thermal Battery Cathodes LiCu$_2$O$_2$ and LiCu$_3$O$_3$ Prepared by a Simple Solid Phase Sintering

Yan Wang[1]*, Xintao Bai[1], Zeshunji Luo[2] and Licai Fu[2]*

[1] The 18th Research Institute of China Electronics Technology Group Corporation, Tianjin, China, [2] College of Material Science and Engineering, Hunan University, Changsha, China

The thermal battery has been designed to be active at high temperature to satisfy storage life and large capacity for storage and emergency power. The development of thermal battery with high specific energy requires that the cathode has high thermal stability and excellent conductivity. Here, the semiconductor material Li–Cu–O compounds LiCu$_2$O$_2$ and LiCu$_3$O$_3$ are synthesized by a simple solid-phase sintering technique, which is simpler than the traditional synthesis process. The thermal decomposition temperatures are 680°C and above 900°C, respectively. This work first applies the Li–Cu–O compounds to the thermal battery. With a cutoff voltage of 1.5 V, the specific capacities of LiCu$_2$O$_2$ and LiCu$_3$O$_3$ are 423 and 332 mA h g^{-1}. Both the decomposition temperature and specific capacity are higher than in the commercial FeS$_2$ and CoS$_2$, especially LiCu$_2$O$_2$. This work affords an alternative of the cathode materials for high specific capacity thermal battery.

Keywords: cathode material, thermal battery, high specific capacity, LiCu$_2$O$_2$, LiCu$_3$O$_3$

INTRODUCTION

The copper-oxide-based material has been investigated as a high-temperature superconductor, LiBs electrode, and catalyst because of its good electrical conductivity, presence of electron holes, and magnetic interactions (Nakamura et al., 2006; Lepple et al., 2017). Of course, copper oxide itself has become the focus of investigations because of its microstructural details, conductivity, and electron structure (Xu et al., 2019). Interest in the system Li–Cu–O also evolved from cathode material for special battery, where a potential usage of Li/CuO thermal battery was considered (Liao et al., 2020). As a primary battery, thermal battery can only be activated when the temperature reached the melting point of eutectic salts electrolyte (Guidotti and Masset, 2006; Masset and Guidotti, 2007; Jeong et al., 2019). This special feature makes the thermal battery have a long shelf-life, excellent mechanical robustness, and being able to supply high output power; it has been used as power sources for guided missiles and proximity fuzes in ordinance devices (Masset and Guidotti, 2007). The cathode materials with poor thermal stability and low specific capacity limit the further development and application of thermal battery.

The Li–Cu–O compounds with a high initial charge capacity are candidates for a new cathode material, such as Li$_2$CuO$_2$ and LiCuO$_2$ (Vitins et al., 2003; Nakamura et al., 2005; Prakash et al., 2005; Arachi et al., 2012; Zhang et al., 2018). Besides, the well-known lithium copper oxides LiCu$_2$O$_2$ and LiCu$_3$O$_3$ with mixed valent copper are unique in the Li–Cu–O system, which gives

rise to high T_c behavior and are semiconductor with ρ_{293K} of 10^6 and $0.1\,\Omega$ cm (Goshall, 1986; Hibble et al., 1990; Roessli et al., 2001; Bush and Kamentsev, 2004; Zhu et al., 2011; Kamentsev et al., 2013; Lepple et al., 2013; Ivanov et al., 2014; Bush et al., 2018). Additionally, $LiCu_2O_2$ and $LiCu_3O_3$ show excellent thermal stability (Hibble et al., 1990; Bush et al., 2004, 2019), which makes them good cathodes for thermal battery. Based on X-ray emission and photoelectron spectra, the valence states of the their Cu atoms are found to be mixed univalent (Cu^I) and divalent (Cu^{II}) (Lin et al., 1996; Zatsepin et al., 1998).

However, it is not easy to obtain a pure single or polycrystalline $LiCu_2O_2$ or $LiCu_3O_3$ phase. CuO, Cu_2O, and Li_2CuO_2 are typical impurities for them (Paszkowicz et al., 2001). Because some Li_2O or Li_2CO_3 are lost during heating, this leads to the formation of CuO and Cu_2O (Hibble et al., 1990). $LiCu_2O_2$ and $LiCu_3O_3$ would be oxidized, forming Li_2CuO_2 at lower temperatures of 310–790°C with oxygen (Bush et al., 2004, 2019). Hence, a majority of synthetic methods for $LiCu_2O_2$ and $LiCu_3O_3$ choose quenching from 800 to 900°C. In addition, homogenizing and reheating are necessary to ensure the uniformity and purity of the product. In order to simplify synthetic methods, the raw materials are mixed by ball mill before being heat treated in this work. Moreover, to keep the high purity, both the synthesis process of $LiCu_2O_2$ and the cooling process of $LiCu_3O_3$ are carried out in Ar. Additionally, the micromorphology of $LiCu_2O_2$ and $LiCu_3O_3$ and their electrochemical performance as cathode materials for thermal batteries were studied.

EXPERIMENTAL

Material Synthesis

All starting materials (**Table 1**) are purchased from commercial sources and used without further purification. Shiny polycrystalline powders of the $LiCu_2O_2$ and $LiCu_3O_3$ are prepared by a simple solid-state method.

As shown in the **Figure 1**, the raw materials for $LiCu_2O_2$, Li_2CO_3, Cu_2O, and CuO are put into an agate jar with agate balls (ball-to-powder weight ratio of 10:1) in a 1:1:2 ratio, and anhydrous ethanol is applied as a solvent. The raw materials are grounded in a ball mill (Tencan powder QXQM-2) for 6 h at a rotation speed of 400 rpm and dried to absolute at 80°C in an air-drying oven (Jinghong DHG-9070A). Subsequently, the mixtures are heat treated at 700°C for 7 h in a tube furnace under flow argon atmospheres with heating and cooling rates of 10°C min^{-1}. In order to synthesize the $LiCu_3O_3$, $Li_2O\cdot4CuO$

is mixed in the same way as raw materials for $LiCu_2O_2$ and then is heat-treated at 880°C for 7 h under flow argon–oxygen mixed atmospheres with heating and cooling rates of 10°C min^{-1} (cooling process only under argon). Dark brown powders of the $LiCu_2O_2$ and black powders of the $LiCu_3O_3$ are ground and keep in air.

Materials Characterization

The phase structures of Li–Cu–O are determined by X-ray diffraction (XRD) on a Mini Flex 600 from 5° (2θ) to 90° (2θ) with Cu-Kα radiation (λ = 0.154178 nm) and X-ray photoelectron spectroscopy (XPS) on a Thermo Fisher Scientific K-ALPHA. For all XRD measurements, the resolution in the scans is kept at 0.01° with a rate of 10° min^{-1}. Thermogravimetric analysis (TG, Henven HCT-4) is conducted with a heating rate of 10°C min^{-1} from room temperature to 900°C and a 50 ml min^{-1} Ar flowrate. The analyses of the microstructures of Li–Cu–O are performed using a scanning electron microscope (SEM, FEI Quanta 200) and a transmission electron microscope (TEM, FEI Tecnai G2 60-300).

Preparation of a Single Thermal Battery Cell and Discharge Test

The single cell was conventionally assembled by lamination. The 0.6 mm Li–B alloy was punched into a disk with a diameter of 17.5 mm as anode. The separator contains 50 wt.% ternary all-lithium eutectic salt electrolyte (LiF–LiCl–LiBr, m.p. = 436°C) and 50 wt.% MgO. Both the cathode (0.15 g Li–Cu–O) and separator were prepared into Φ 17.5 mm by powder tableting process. The cell was assembled in a glove box with the water and oxygen content being <5 ppm.
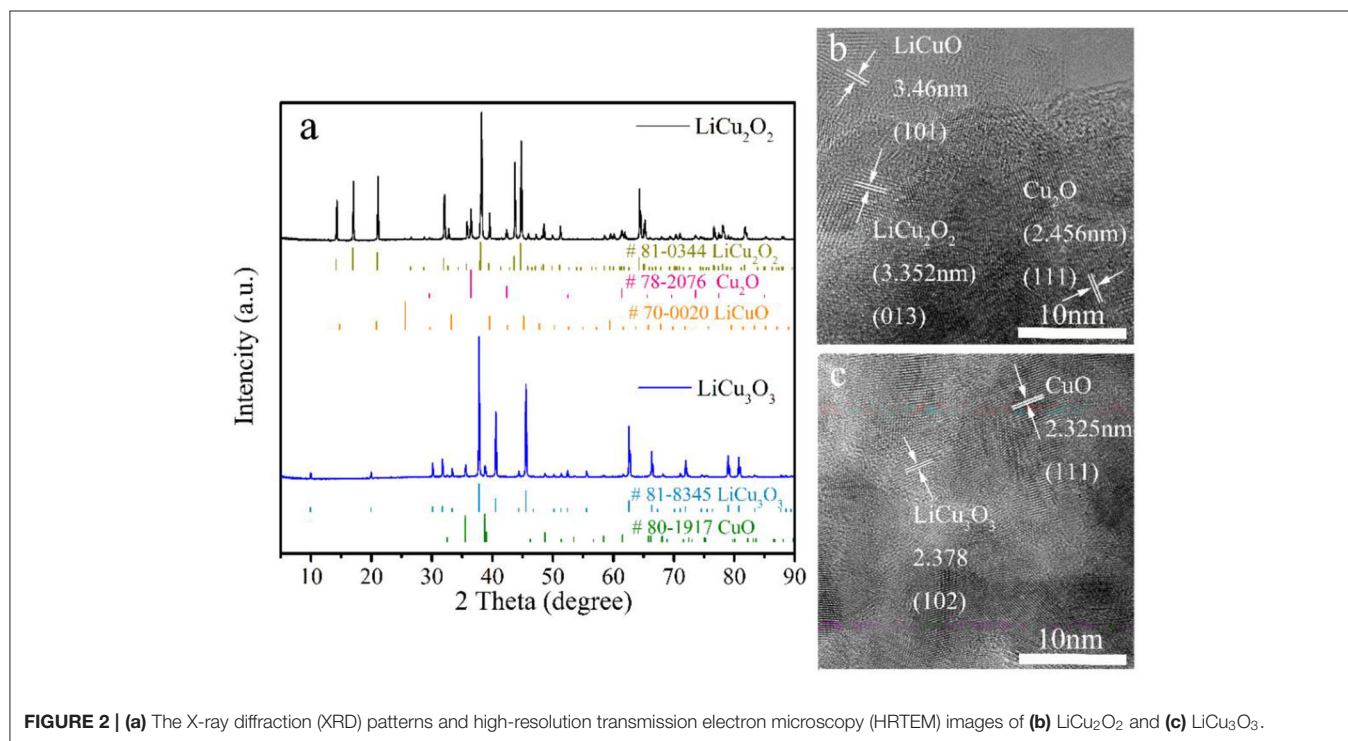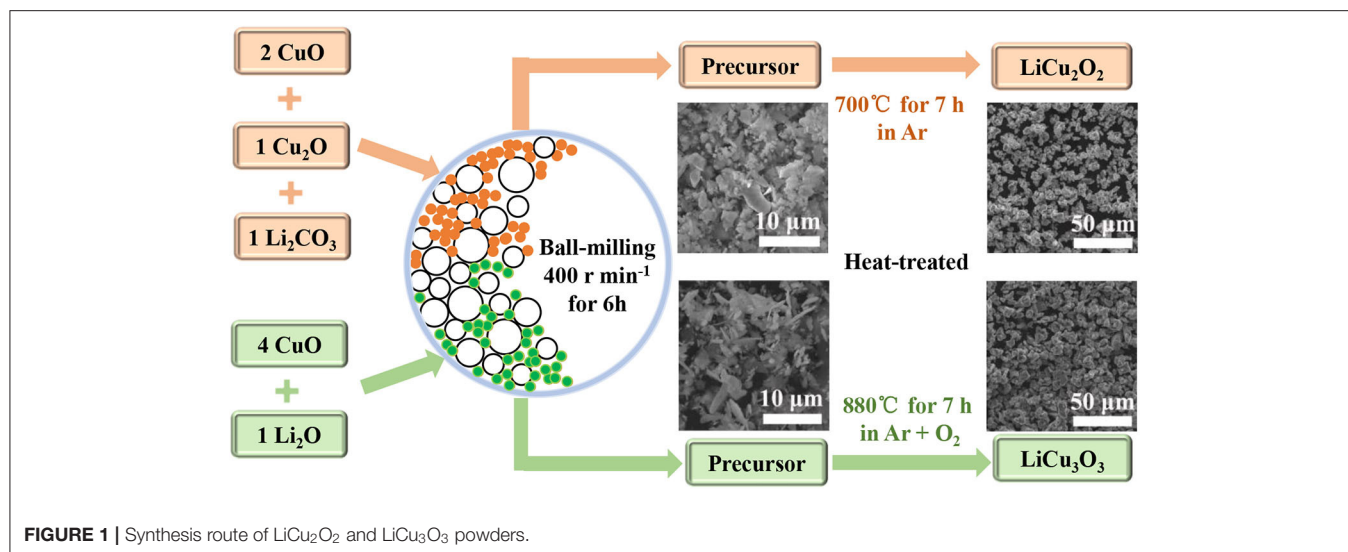
Discharge performances are evaluated on an IT8511 plus the single-channel programmable electronic load (ITECH). The single cell was sandwiched between two collectors. Before the tests, the temperature-controlled stainless steel cylinder heater was heated from room temperature to 500°C. The discharge current density is 0.1 A cm^{-2} with the cutoff voltage of 1.5 V (75% of the peak voltage) at 500°C.

RESULTS AND DISCUSSION

The XRD patterns of both powders closely agreed with $LiCu_2O_2$ (#81-0344) and $LiCu_3O_3$ (#81-0345), respectively (**Figure 2**). The as-grown crystals contain only traces of foreign phases (LiCuO, Cu_2O, and CuO). The purity of the quantitative analysis of the powder diffraction patterns are 93.1 wt.% $LiCu_2O_2$ and 93.7 wt.% $LiCu_3O_3$, which were calculated by K value method according to **Table 2**. The reason why impurity phase such as Cu_2O or CuO existed on samples may be the loss of Li_2CO_3 or Li_2O during prolonged heating (Hibble et al., 1990), while the LiCuO can be attributed to the uncomplete reaction during synthesis process. The high-resolution transmission electron microscopy (HRTEM) presented that the main composition is $LiCu_2O_2$ or $LiCu_3O_3$ (**Figures 2b,c**). A few retained phases, such as CuO, and Cu_2O, can also be detected. These results verified that $LiCu_2O_2$ and $LiCu_3O_3$ were prepared successfully.

TABLE 1 | Chemical reagents used in the experiment.

Name	Molecular formula	Particle size	Purity	Manufacturer
Copper oxide	CuO	1–30 μm	99.00%	Sinopharm
Cuprous oxide	Cu_2O	1–5 μm	99.00%	Macklin
Lithium carbonate	Li_2CO_3	5–20 μm	99.00%	Aladdin
Lithium oxide	Li_2O	5–50 μm	99.99%	Aladdin

FIGURE 1 | Synthesis route of LiCu₂O₂ and LiCu₃O₃ powders.

FIGURE 2 | (a) The X-ray diffraction (XRD) patterns and high-resolution transmission electron microscopy (HRTEM) images of **(b)** LiCu₂O₂ and **(c)** LiCu₃O₃.

The chemical state of LiCu₂O₂ and LiCu₃O₃ was studied using XPS (**Figures 3A–F**). Their XPS core-level spectra of Cu 2p comprise intense spin-orbit split peaks for 2p 3/2 (934.1 eV) and 2p 1/2 (954.2 eV) accompanied by satellite peaks (939–945 eV and 959–964 eV), which are typical of Cu^{II} valency (Zatsepin et al., 1998; Momeni and Sedaghati, 2018). Besides, the remaining two main fitted peaks center at 932.4 and 952.5 eV, representing Cu 2p3/2 and Cu 2p1/2 of Cu^{I}, respectively (Wang et al., 2018; Zhou et al., 2018). The O 1s peaks located at binding energies of 531.1 and 531.6 eV are in good agreement with the reported values of Cu₂O and CuO, respectively (Han et al., 2018). According to the XRD patterns (**Figure 2a**), the impurity phases of synthesized LiCu₂O₂ and LiCu₃O₃ are Cu₂O and CuO, respectively. Thus, Cu^{II} in LiCu₂O₂ and Cu^{I} in LiCu₃O₃ can only come from themselves. To sum up, the coexistence of Cu^{I} and Cu^{II} ions in LiCu₂O₂ and LiCu₃O₃ can be concluded.

The LiCu₂O₂ consisted of many uniform distributed clusters with an average size of about 1 μm (**Figure 4a**), which increased the compaction density of the cathode. The local high magnification showed that these clusters were composed of LiCu₂O₂ nanograins and impurity-phase Cu₂O (**Figures 2b, 4b**).
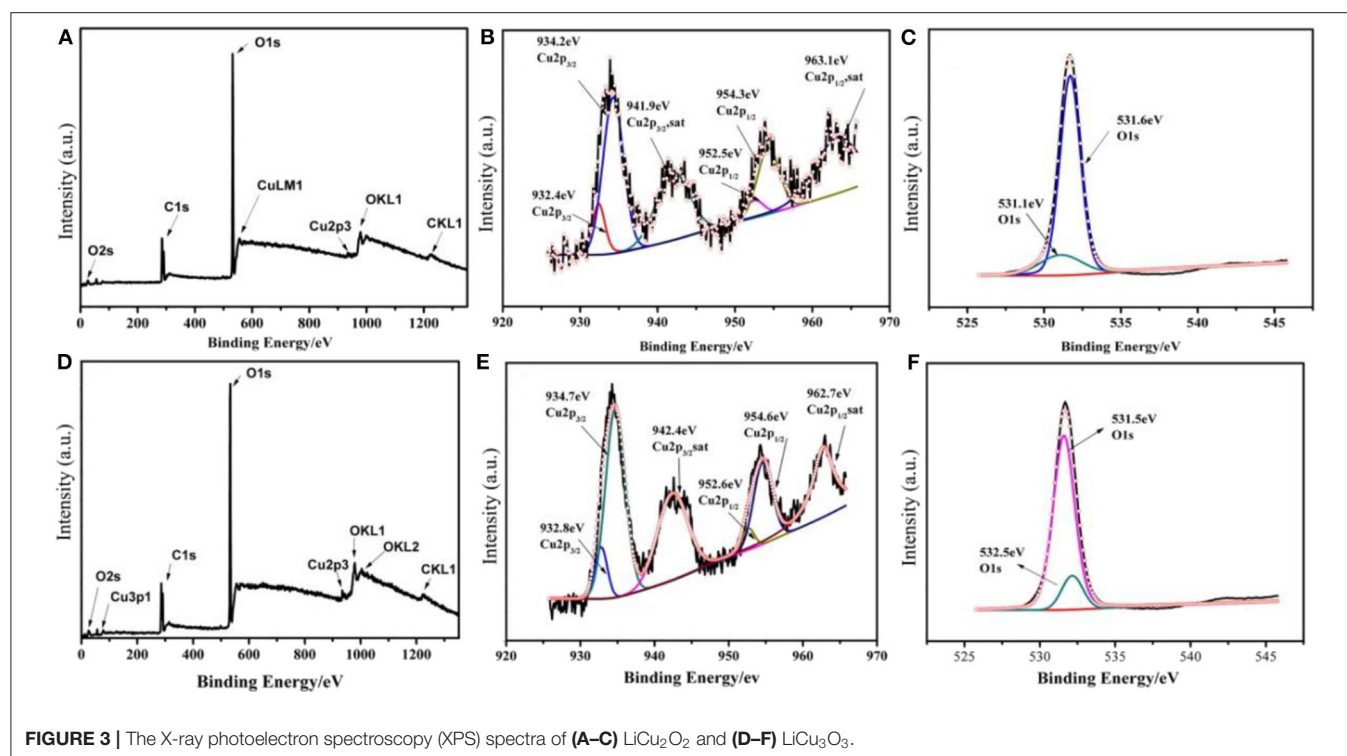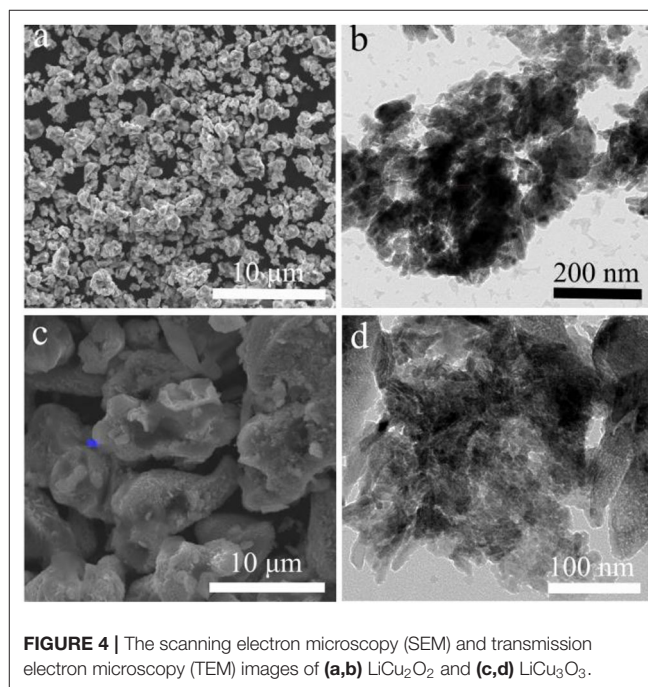
FIGURE 3 | The X-ray photoelectron spectroscopy (XPS) spectra of **(A–C)** LiCu$_2$O$_2$ and **(D–F)** LiCu$_3$O$_3$.

TABLE 2 | The information of X-ray diffraction (XRD) patterns of synthesized LiCu$_2$O$_2$ and LiCu$_3$O$_3$.

	RIR	I (a.u.)	W (wt.%)
LiCu$_2$O$_2$	3.01	14,962	93.1
Cu$_2$O	8.28	2,815	6.4
LiCuO	3.57	96	0.5
LiCu$_3$O$_3$	3.37	18,979	93.7
CuO	3.9	1,483	6.3

Both the statistical data and the XRD pattern indicated that the average grain size is about 40 nm, which is beneficial to shortening the migration path of lithium ion, while the roughness surface of clusters could improve the activation sites of the electrochemical reaction and contact area between the cathode and fusional electrolyte. The roughness of the particle might be caused by the composition of nanograins. However, the cluster size of LiCu$_3$O$_3$ increased to 2–15 μm, which were composed of 20–200 nm grains (**Figures 4c,d**). This size distribution range was far larger than LiCu$_2$O$_2$. Thus, it could be expected that the discharge performance of LiCu$_2$O$_2$ would be more excellent than that of LiCu$_3$O$_3$.

Thermal stability is one of the important indicators for thermal battery cathode (Jin et al., 2018; Luo et al., 2020). As shown in **Figure 5A**, LiCu$_2$O$_2$ began to decompose to LiCuO, Cu$_2$O, and O$_2$ at around 680°C. The weight loss at 380°C was about 1.81%, which was mainly caused by the decomposition of Li$_2$CO$_3$. Due to the lower content and poor

FIGURE 4 | The scanning electron microscopy (SEM) and transmission electron microscopy (TEM) images of **(a,b)** LiCu$_2$O$_2$ and **(c,d)** LiCu$_3$O$_3$.

crystallinity, the auxiliary material Li$_2$CO$_3$ could not be detected in XRD. Since there is no Li$_2$CO$_3$ as the reactant, this weight loss peak cannot be observed in the TG curve of LiCu$_3$O$_3$ (**Figure 5B**). Unlike the LiCu$_2$O$_2$, the LiCu$_3$O$_3$ was kept stable below 900°C with a weight loss <1.0%. In summary, both of them
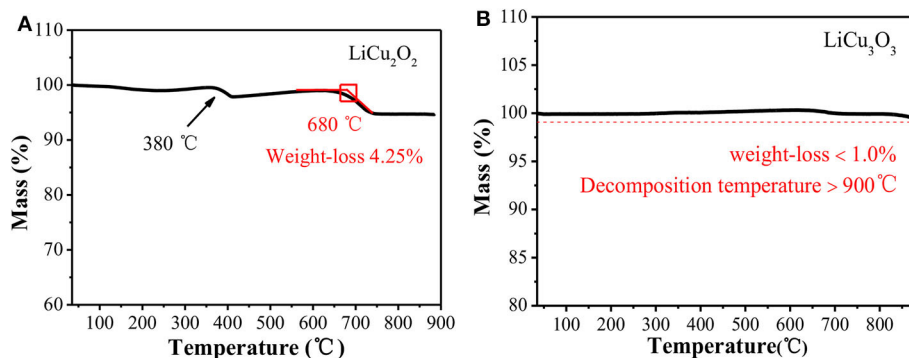
FIGURE 5 | The thermogravimetric analysis (TG) curves of LiCu$_2$O$_2$ **(A)** and LiCu$_3$O$_3$ **(B)**.
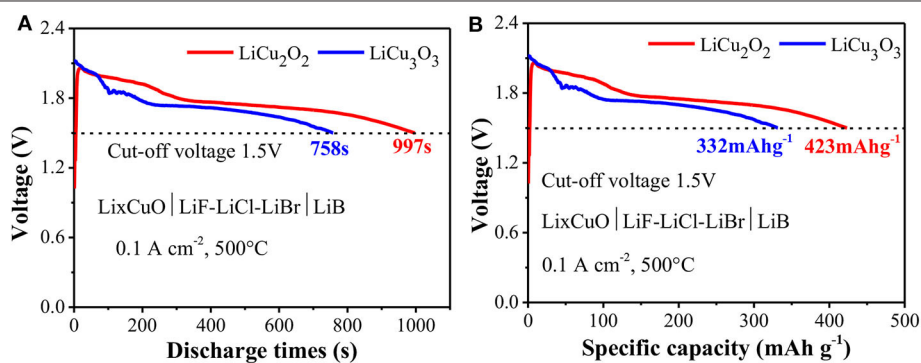

FIGURE 6 | The discharge curves of LiCu$_2$O$_2$ **(A)** and LiCu$_3$O$_3$ **(B)**.
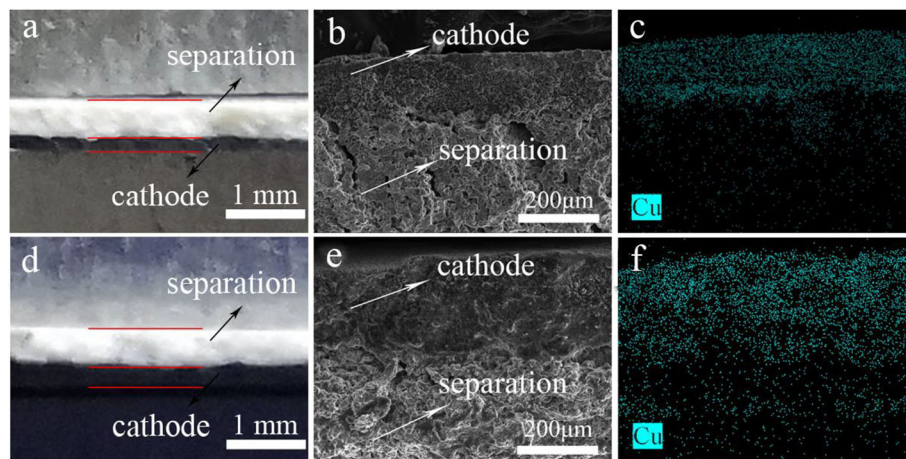

FIGURE 7 | The images of cathode and electrolyte before discharge, cross-sectional SEM image, and corresponding Cu distribution of thermal battery after discharge: **(a–c)** LiCu$_2$O$_2$ and **(d–f)** LiCu$_3$O$_3$.

have great thermal stability compared with the conventional thermal battery cathodes, such as FeS$_2$ and CoS$_2$ (Masset and Guidotti, 2008). The high temperature stability completely satisfied the temperature requirements of thermal battery during actual discharge.

The LiCu$_2$O$_2$ and LiCu$_3$O$_3$ presented excellent electrochemical performance (**Figure 6**). The voltage of LiCu$_2$O$_2$ quickly increased to a peak value of 2.06 V once the thermal battery is activated, in which the impurity phase Cu$_2$O of LiCu$_2$O$_2$ might belong. It is below 2–3 s, which is far shorter than

in the secondary Li^+ or Li metal battery during larger current discharge. The relative steady voltage platforms were 1.95 and 1.72 V, which were about 0.4 V lower than the theoretical values (Patat et al., 1991; Lepple et al., 2013) due to the resistance of the actual discharge. The voltage of $LiCu_2O_2$ gradually decreased along with three steps during discharge. The $LiCu_3O_3$ also showed similar discharge characterizations. It should be noted that the peak voltage of $LiCu_3O_3$ reached about 2.12 V. This high voltage spike is shown by the raw material CuO, which was significantly enhanced in $LiCu_3O_3$ during the initial discharge (Liao et al., 2020). The discharge time is the key factor to the practical application of thermal battery in the field of defense. In this case, the discharge time of $LiCu_2O_2$ reached 997 s with high cutoff voltage of 1.5 A at large current density of 0.1 A cm^{-2}. The corresponding specific capacity was 423 mA h g^{-1}. Since the $LiCu_3O_3$ particle has a large size and ununiform distribution, it showed a lower specific capacity of 332 mA h g^{-1}, but it is still higher than that of commercial FeS_2 of 210 mA h g^{-1} and CoS_2 of 250 mA h g^{-1}. Both $LiCu_2O_2$ and $LiCu_3O_3$ have excellent conductivity and thermal stability.

After discharge, the cross-section between $LiCu_2O_2$ and electrolyte showed relatively clear interface and particle characters (**Figures 7a,b**). The Cu elemental mapping also indicated that few Cu diffused from the cathode into the electrolyte (**Figure 7c**). This interface for $LiCu_3O_3$ thermal battery became blurry, and some Cu can be detected into the electrolyte (**Figures 7d–f**). The thickness of $LiCu_3O_3$ cathode varies more than that of $LiCu_2O_2$ cathode. This phenomenon is known in thermal battery as high solubility in molten salt, which degrades the battery's performance (Jin et al., 2017). For this reason, the performance of $LiCu_3O_3$ thermal battery is worse than that of $LiCu_2O_2$ thermal battery. It is demonstrated that $LiCu_2O_2$ could keep the structure at high temperature instead of being molten, forming blurry interface for $LiCu_3O_3$. To sum up, their discharge performance, especially for $LiCu_2O_2$ cathode, provides a new idea for improving the specific capacity of CuO and Cu_2O. $LiCu_2O_2$ and $LiCu_3O_3$ are suitable for use as cathode materials for thermal battery with long life and high specific capacity.

CONCLUSIONS

The thermal battery is a kind of Li metal primary battery. The characteristics of high temperature, large current, and long working life of the cathode material require it to have high temperature stability and high specific capacity. In this paper, high-purity $LiCu_2O_2$ and $LiCu_3O_3$ were synthesized by combining simple mechanical ball mill and solid-phase sintering technique. By considering the excellent thermal stability and high specific capacity for both $LiCu_2O_2$ and $LiCu_3O_3$, this work developed two new cathode materials for thermal battery ($LiCu_2O_2$ or $LiCu_3O_3|LiF-LiCl-LiBr|LiB$). The electrochemical tests showed that both cathodes exhibited excellent specific capacity. Especially for the $LiCu_2O_2$, the actual specific energy was up to 423 mA h g^{-1} with cutoff voltage of 1.5 V at 0.1 A cm^{-2} and 500°C. It was higher than the commercial thermal battery cathodes such as FeS_2 and CoS_2. This paper indicates that $LiCu_2O_2$ and $LiCu_3O_3$ are promising cathode materials with the high specific capacity for thermal battery.

DATA AVAILABILITY STATEMENT

The raw data supporting the conclusions of this article will be made available by the authors, without undue reservation.

AUTHOR CONTRIBUTIONS

YW and LF contributed to conception and design of the study. ZL and LF organized the database. YW and XB performed the statistical analysis. YW wrote the first draft of the manuscript. XB, ZL, and LF wrote sections of the manuscript. All authors contributed to manuscript revision, read, and approved the submitted version.

FUNDING

REFERENCES

Arachi, Y., Setsu, T., Ide, T., Hinoshita, K., and Nakata, Y. (2012). Reversible electrochemical reaction of CuO with Li in the LiCuO2 system. *Solid State Ion.* 225, 611–614. doi: 10.1016/j.ssi.2011.12.006

Bush, A. A., Buettgen, N., Gippius, A. A., Horvatic, M., Jeong, M., Kraetschmer, W., et al. (2018). Exotic phases of frustrated antiferromagnet LiCu2O2. *Phys. Rev. B* 97:054428. doi: 10.1103/PhysRevB.97.054428

Bush, A. A., and Kamentsev, K. E. (2004). Electrical instability of LiCu2O2 crystals. *Phys. Solid State* 46, 445–452. doi: 10.1134/1.1687858

Bush, A. A., Kamentsev, K. E., and Tishchenko, E. A. (2004). Crystal growth, thermal stability, and electrical properties of LiCu2O2. *Inorg. Mater.* 40, 44–49. doi: 10.1023/B:INMA.0000012177.38378.10

Bush, A. A., Kamentsev, K. E., and Tishchenko, E. A. (2019). Growth, thermogravimetric characterization, and electrical properties of LiCu3O3 single crystals. *Inorg. Mater.* 55, 374–379. doi: 10.1134/S0020168519040046

Goshall, N. A. (1986). Lithium transport in ternary lithium-copper-oxygen cathode materials. *Solid State Ion.* 18-19, 788–793. doi: 10.1016/0167-2738(86)90263-8

Guidotti, R. A., and Masset, P. (2006). Thermally activated ("thermal") battery technology_ part I_ an overview. *J. Power Sources* 161, 1443–1449. doi: 10.1016/j.jpowsour.2006.06.013

Han, X., He, X., Sun, L., Han, X., Zhan, W., Xu, J., et al. (2018). Increasing effectiveness of photogenerated carriers by *in situ* anchoring of Cu2O nanoparticles on a nitrogen-doped porous carbon yolk–shell cuboctahedral framework. *ACS Catal.* 8, 3348–3356. doi: 10.1021/acscatal.7b04219

Hibble, S. J., Köhler, J., and Simon, A. (1990). LiCu2O2 and LiCu3O3_ new mixed valent copper oxides. *J. Solid State Chem.* 88, 534–542. doi: 10.1016/0022-4596(90)90251-R

Ivanov, S. A., Anil Kumar, P., Mathieu, R., Bush, A. A., Ottosson, M., and Nordblad, P. (2014). Temperature evolution of structural and magnetic properties of stoichiometric LiCu2O2: correlation of thermal expansion coefficient and magnetic order. *Solid State Sci.* 34, 97–101. doi: 10.1016/j.solidstatesciences.2014.05.014

Jeong, M. G., Cho, J.-H., and Lee, B. J. (2019). Heat transfer analysis of a high-power and large-capacity thermal battery and investigation of effective thermal model. *J. Power Sources* 424, 35–41. doi: 10.1016/j.jpowsour.2019.03.067

Jin, C., Fu, L., Zhu, J., Yang, W., Li, D., and Zhou, L. (2018). A hierarchical carbon modified nano-NiS2 cathode with high thermal stability for a high energy thermal battery. *J. Mater. Chem. A* 6, 7123–7132. doi: 10.1039/C8TA00346G

Jin, C., Zhou, L., Fu, L., Zhu, J., and Li, D. (2017). Synthesis and discharge performances of NiCl2 by surface modification of carbon coating as cathode material of thermal battery. *Appl. Surf. Sci.* 402, 08–313. doi: 10.1016/j.apsusc.2017.01.034

Kamentsev, K. E., Bush, A. A., Tishchenko, E. A., Ivanov, S. A., Ottoson, M., Mathieu, R., et al. (2013). High-temperature structural phase transition in the LiCu2O2 multiferroic. *J. Exp. Theor. Phys.* 117, 320–326. doi: 10.1134/S1063776113100026

Lepple, M., Adam, R., Cupid, D. M., Franke, P., Bergfeldt, T., Wadewitz, D., et al. (2013). Thermodynamic investigations of copper oxides used as conversion type electrodes in lithium ion batteries. *J. Mater. Sci.* 48, 5818–5826. doi: 10.1007/s10853-013-7374-x

Lepple, M., Rohrer, J., Adam, R., Cupid, D. M., Rafaja, D., Albe, K., et al. (2017). Thermochemical stability of Li-Cu-O ternary compounds stable at room temperature analyzed by experimental and theoretical methods. *Int. J. Mater. Res.* 108, 959–970. doi: 10.3139/146.111560

Liao, Z., Fu, L., Zhu, J., Yang, W., Li, D., and Zhou, L. (2020). High specific energy flexible CuO thin film cathode for thermal batteries. *J. Power Sources* 463:228237. doi: 10.1016/j.jpowsour.2020.228237

Lin, J. H., Li, K., Ruan, S. K., and Su, M. Z. (1996). Thermostability OF LiCu2O2 and LiCu3O3. *Chin. Chem. Lett.* 7, 195–198.

Luo, Z., Fu, L., Zhu, J., Yang, W., Li, D., and Zhou, L. (2020). Cu2O as a promising cathode with high specific capacity for thermal battery. *J. Power Sources* 448:227569. doi: 10.1016/j.jpowsour.2019.227569

Masset, P., and Guidotti, R. A. (2007). Thermal activated (thermal) battery technology_ part II. molten salt electrolytes. *J. Power Sources* 164 397–414. doi: 10.1016/j.jpowsour.2006.10.080

Masset, P. J., and Guidotti, R. A. (2008). Thermal activated ("thermal") battery technology Part III. cathode materials. *J. Power Sources* 177, 595–609. doi: 10.1016/j.jpowsour.2007.11.017

Momeni, S., and Sedaghati, F. (2018). CuO/Cu2O nanoparticles: a simple and green synthesis, characterization and their electrocatalytic performance toward formaldehyde oxidation. *Microchem. J.* 143, 64–71. doi: 10.1016/j.microc.2018.07.035

Nakamura, K., Kawai, K., Yamada, K., Michihiro, Y., Moriga, T., Nakabayashi, I., et al. (2006). Li+ ionic diffusion in Li-Cu-O compounds. *Solid State Ion.* 177, 2775–2778. doi: 10.1016/j.ssi.2006.03.046

Nakamura, K., Moriga, T., Sumi, A., Kashu, Y., Michihiro, Y., Nakabayashi, I., et al. (2005). NMR study on the Li+ ion diffusion in LiCuO2 with layered structure. *Solid State Ion.* 176, 837–840. doi: 10.1016/j.ssi.2004.11.004

Paszkowicz, W., Marczak, M., Vorotynov, A. M., Sablina, K. A., and Petrakovskii, G. A. (2001). Powder diffraction study of LiCu2O2 crystals. *Powder Diffr.* 16, 30–36. doi: 10.1154/1.1314389

Patat, S., Blunt, D. P., and Chippindale, A. M., Dickens, P. G. (1991). The thermochemistry of LiCuO, Li2CuO 2 and LiCu2O2. *Solid State Ion.* 46, 325–329. doi: 10.1016/0167-2738(91)90233-2

Prakash, A. S., Larcher, D., Morcrette, M., Hegde, M. S., Leriche, J. B., and Masquelier, C. (2005). Synthesis, phase stability, and electrochemically driven transformations in the LiCuO2-Li2CuO2 system. *Chem. Mater.* 17, 4406–4415. doi: 10.1021/cm0508266

Roessli, B., Staub, U., Amato, A., Herlach, D., Pattison, P., Sablina, K., et al. (2001). Magnetic phase transitions in the double spin-chains compound LiCu2O2. *Physica B Condens. Matter* 296, 306–311. doi: 10.1016/S0921-4526(00)00574-3

Vitins, G., Raekelboom, E. A., Weller, M. T., and Owen, J. R. (2003). Li2CuO2 as an additive for capacity enhancement of lithium ion cells. *J. Power Sources* 119-121, 938–942. doi: 10.1016/S0378-7753(03)00236-2

Wang, C. L., Tissot, H., Escudero, C., Perez-Dieste, V., Stacchiola, D., and Weissenrieder, J. (2018). Redox properties of Cu2O(100) and (111) surfaces. *J. Phys. Chem. C* 122, 28684–28691. doi: 10.1021/acs.jpcc.8b08494

Xu, C., Manukyan, K. V., Adams, R. A., Pol, V. G., Chen, P., and Varma, A. (2019). One-step solution combustion synthesis of CuO/Cu2O/C anode for long cycle life Li-ion batteries. *Carbon* 142, 51–59. doi: 10.1016/j.carbon.2018.10.016

Zatsepin, D. A., Galakhov, V. R., Korotin, M. A., Fedorenko, V. V., and Kurmaev, E. Z. (1998). Valence states of copper ions and electronic structure of LiCu2O2. *Phys. Rev. B* 57, 4377–4381. doi: 10.1103/PhysRevB.57.4377

Zhang, S. S., Fan, X., and Wang, C. (2018). An *in-situ* enabled lithium metal battery by plating lithium on a copper current collector. *Electrochem. Commun.* 89, 23–26. doi: 10.1016/j.elecom.2018.02.011

Zhou, T., Zang, Z., Wei, J., Zheng, J., Hao, J., Ling, F., et al. (2018). Efficient charge carrier separation and excellent visible light photoresponse in Cu2O nanowires. *Nano Energy* 50, 118–125. doi: 10.1016/j.nanoen.2018.05.028

Zhu, X., Yao, Y., Hsu, H. C., Chou, F. C., and El-Batanouny, M. (2011). Temperature-dependent anomalies in the structure of the (001) surface of LiCu2O2. *Surf. Sci.* 605, 376–382. doi: 10.1016/j.susc.2010.11.004